Available online at www.sciencedirect.com

SciVerse ScienceDirect

journal homepage: www.elsevier.com/locate/watres

Roles of ionic strength and biofilm roughness on adhesion kinetics of *Escherichia coli* onto groundwater biofilm grown on PVC surfaces

Dao Janjaroen [a], *Fangqiong Ling* [a], *Guillermo Monroy* [b], *Nicolas Derlon* [d], *Eberhard Mogenroth* [d,e], *Stephen A. Boppart* [b,c], *Wen-Tso Liu* [a], *Thanh H. Nguyen* [a,*]

[a] *Department of Civil and Environmental Engineering, University of Illinois at Urbana-Champaign, Urbana, IL 61801, USA*
[b] *Department of Bioengineering, University of Illinois at Urbana-Champaign, Urbana IL 61801, USA*
[c] *Department of Electrical and Computer Engineering, University of Illinois at Urbana-Champaign, Urbana, IL 61801, USA*
[d] *Eawag: Swiss Federal Institute of Aquatic Science and Technology, 8600 Dübendorf, Switzerland*
[e] *ETH Zürich, Institute of Environmental Engineering, 8093 Zürich, Switzerland*

ARTICLE INFO

Article history:
Received 21 August 2012
Received in revised form
11 February 2013
Accepted 12 February 2013
Available online 26 February 2013

Keywords:
Drinking water distribution system
Biofilm
Pathogens

ABSTRACT

Mechanisms of *Escherichia coli* attachment on biofilms grown on PVC coupons were investigated. Biofilms were grown in CDC reactors using groundwater as feed solution over a period up to 27 weeks. Biofilm physical structure was characterized at the micro- and meso-scales using Scanning Electron Microscopy (SEM) and Optical Coherence Tomography (OCT), respectively. Microbial community diversity was analyzed with Terminal Restricted Fragment Length Polymorphism (T-RFLP). Both physical structure and microbial community diversity of the biofilms were shown to be changing from 2 weeks to 14 weeks, and became relatively stable after 16 weeks. A parallel plate flow chamber coupled with an inverted fluorescent microscope was also used to monitor the attachment of fluorescent microspheres and *E. coli* on clean PVC surfaces and biofilms grown on PVC surfaces for different ages. Two mechanisms of *E. coli* attachment were identified. The adhesion rate coefficients (k_d) of *E. coli* on nascent PVC surfaces and 2-week biofilms increased with ionic strength. However, after biofilms grew for 8 weeks, the adhesion was found to be independent of solution chemistry. Instead, a positive correlation between k_d and biofilm roughness as determined by OCT was obtained, indicating that the physical structure of biofilms could play an important role in facilitating the adhesion of *E. coli* cells.

1. Introduction

Biofilms are aggregates of cells and extracellular polymeric substances (EPS), and are found ubiquitously in both natural and engineered systems, such as on a pipe surface in Drinking Water Distribution Systems (DWDS) (Berry et al., 2006; Flemming and Wingender, 2010). Biofilms in DWDS were reported to be capable of attracting and harboring pathogens (Berry et al., 2006). In addition, biofilm matrix may prevent disinfectants from reaching the cells located deep inside the biofilm (Berry et al., 2009; Gagnon et al., 2008; Norton et al., 2004; Williams and Braun-Howland, 2003). As a result,

* *Corresponding author*. Tel.: +1 217 244 5965; fax: +1 217 333 6968.
E-mail addresses: djanjar2@illinois.edu (D. Janjaroen), ling5@illinois.edu (F. Ling), gmonroy2@illinois.edu (G. Monroy), nicolas.derlon@eawag.ch (N. Derlon), eberhard.morgenroth@eawag.ch (E. Mogenroth), boppart@illinois.edu (S.A. Boppart), wtliu@illinois.edu (W.-T. Liu), thn@illinois.edu, thn@uiuc.edu (T.H. Nguyen).
0043-1354/$ – see front matter © 2013 Elsevier Ltd. All rights reserved.
http://dx.doi.org/10.1016/j.watres.2013.02.032

pathogenic microorganisms such as *Mycobacterium avium* and *Legionella pneumophila* have been found in DWDS biofilms (Falkinham et al., 2001; Le Dantec et al., 2002; Torvinen et al., 2004; Declerck et al., 2009; Lau and Ashbolt, 2009; Valster et al., 2011; Wullings et al., 2011). More importantly, pathogen presence and survival in DWDS has been linked to outbreaks (Craun et al., 2010, 1998, 2002). Thus, understanding the mechanisms of pathogen attachment to biofilms developed in DWDS is of crucial interest to ensure the quality of the drinking water.

While previous studies have convincingly presented the evidence that biofilms can harbor pathogens (Flemming and Wingender, 2010; Altman et al., 2009; Helmi et al., 2010, 2008; Kumar and Anand, 1998), systematic studies to identify the physical and chemical factors controlling pathogen attachment to biofilm are rare. For example, *Escherichia coli* and fluorescent polystyrene beads have been found to attach more to biofilms grown from tap water on glass slides than to the surface of clean glass slides (Paris et al., 2009). Biofilm characteristics such as age and coverage have been identified as controlling factors for *E. coli* and microsphere attachment (Paris et al., 2009, 2007). In contrast, attachment of *Legionella*, bacteriophages, and microspheres on biofilms grown from lake water on glass surface was found to be independent of biofilm cell surface density, but dependent on particle surface properties, such as hydrophobicity (Långmark et al., 2005). Spatial distribution of biofilms but not their cell density was found to be dependent on the wall shear rate (Paris et al., 2007). It is likely that under different shear rates, biofilms can develop into different physical structures. Biofilm roughness has been found to control deposition of *Cryptosporidium* oocysts and *E. coli* to *Pseudomonas aeruginosa* biofilms (Searcy et al., 2006; Wu et al., 2012). Roughness of mixed-species river biofilms was also found to control oocyst deposition (DiCesare et al., 2012). The first step of biofilm formation involving bacterial cell adhesion to surface has been studied in much more detail than adhesion of cells to mature biofilms. Interactions including electrostatic, van der Waals, acid-base, hydrophobic, and steric, have been found to control this first step of biofilm formation, as reviewed by Karunakaran et al. (2011). However, a systematic study on the roles of biofilm age, and biofilm physical structure on bacterial cell attachment to mixed-culture biofilms grown on pipe materials has not been conducted.

Our study aims to elucidate the mechanisms that govern the attachment of *E. coli* S17 to groundwater biofilms grown on PVC surfaces. Specifically, we will focus on the role of water chemistry and biofilm structure on *E. coli* attachment. We use *E. coli* S17 as a surrogate of bacterial pathogens because deposition of *E. coli* to the biofilms represents intrusion of biological contaminants into DWDS. The advantages of using groundwater, which is the source for drinking water in the Champaign-Urbana area, include a stable chemistry, disinfectant free and higher carbon source, allowing faster biofilm growth. A parallel plate flow chamber (PPFC) was used to monitor attachment of *E. coli* onto clean PVC surfaces and biofilm grown on PVC. Physical and biological characterization of groundwater biofilm was used to explain attachment mechanisms. Multi-species biofilms were grown from groundwater on PVC pipe coupons for up to 25 weeks. Biofilm development was studied through a combination of microbial community analysis and quantitative determination of biofilm thickness and roughness. The latter was determined by OCT, instead of conventional confocal scanning laser microscopy (CSLM) because of the thicker biofilm grown on the non-transparent surface used in this study. Advantages of OCT over CSLM typically include the ability to image deeper in thicker, highly scattering biofilms, and the ability to image over larger areas and volumes (Derlon et al., 2012; Haisch and Niessner, 2007; Nguyen et al., 2012, 2010; Xi et al., 2006). Specifically in this study, OCT was used to image biofilm areas of 1 mm × 2 mm and biofilms thicker than 25 μm. In addition, OCT does not require the biofilm to be stained. In this study, the composition of the biofilms grown from groundwater was unknown, and staining would only provide image contrast for only a portion of the biofilm.

2. Materials and methods

2.1. Bacteria cell preparation

E. coli (*E. coli* S17-1 λ-pir) was obtained from Dr. Thomas at the University of Wisconsin (Simon et al., 1983). This *E. coli* was tagged with Green Fluorescing Protein (GFP) plasmid. Preparation of *E. coli* cells for adhesion experiments is documented in the Supplementary materials.

2.2. Biofilm preparation

A CDC reactor (CBR 90-2) was obtained from BioSurface Technologies Corporation and was used to grow biofilm on PVC coupons (RD 128-PVC). PVC coupons were secured to plastic rods in the reactor. Groundwater collected from a natural aquifer underneath the Newmark Civil Engineering Laboratory (205 N. Matthews, Urbana, Illinois, 61801) was first treated with a greensand filter to remove iron and manganese. This groundwater was well characterized and used in previous studies (Bradley et al., 2011; Li et al., 2002). The chemical characteristics of the groundwater including alkalinity, hardness and trace metals, were analyzed by the Illinois State Water Survey. Groundwater was collected into a reservoir every 2 days and was continuously pumped through the reactor at a flow rate of 1.30 mL/min corresponding to a hydraulic retention time of 4 h. Mixing of the bulk liquid was performed using a magnetic stirrer at 125 rpm. Biofilms were grown to different ages from 2 to 27 weeks.

2.3. Contact angle measurement and surface energy estimation

Contact angle measurements of *E. coli*, biofilm, and PVC were measured by static sessile drop technique using a Goniometer (KSV Instrument, CAM 200). Diiodomethane, which is non-polar and hydrophobic, was used as a probe liquid in contact angle measurements. The contact angle between diiodomethane and the surface was used to calculate the Lifshitz–van der Waals (γ^{LW}) component of surface energy (Brant and Childress, 2002; van Oss, 1993; van der Mei et al., 1998; Zaidi et al., 2011; Busscher et al., 1984). A layer of *E. coli*

Table 1 – Contact angle and corresponding Hamaker's constant (A) of biofilms (BF), PVC, CML, and *E. coli* using diiodomethane as a liquid probe. Contact angles were measured by sessile drop using goniometer. Hamaker's constant was calculated from contact angle.

	$\Theta_{diiodomethane}$	γ^{LW} (mJ/m^2)	ΔG (mJ/m^2)	A (J)
PVC	49.8 ± 2.2	34		
Biofilm 2 wk	43.2 ± 1.5	38		
Biofilm 4 wk	34.5 ± 1.3	42		
Biofilm 6 wk	36.3 ± 2.3	41		
Biofilm 8 wk	35.0 ± 4.7	42		
Biofilm 16 wk	33.7 ± 2.9	42.6		
Biofilm 24 wk	26.6 ± 2.9	45.6		
Biofilm 27 wk	26 ± 1.0	45		
E.coti S17	70.6 ± 2.2	22		
CML	55.1 ± 2	31.3		
CML – water – PVC			-6.6×10^{-4}	6.1×10^{-22}
CML – water – BF 2 wk			-5.0×10^{-4}	4.6×10^{-22}
CML – water – BF 4 wk			-3.4×10^{-4}	3.2×10^{-22}
CML – water – BF 8 wk			-3.4×10^{-4}	3.2×10^{-22}
CML – water – BF 16 wk			-3.2×10^{-4}	3.0×10^{-22}
CML – water – BF 24 wk			-2.0×10^{-4}	1.9×10^{-22}
CML – water – BF 27 wk			-2.3×10^{-4}	2.1×10^{-22}
E. coli – water – PVC			-1.6×10^{-3}	1.5×10^{-21}
E. coli – water – BF 2 wk			-1.3×10^{-3}	1.2×10^{-21}
E. coli – water – BF 4 wk			-1.1×10^{-3}	9.8×10^{-22}
E. coli – water – BF 6 wk			-1.1×10^{-3}	1.0×10^{-21}
E. coli – water – BF 8 wk			-1.1×10^{-3}	9.8×10^{-22}
E. coli – water – BF 16 wk			-1.1×10^{-3}	9.8×10^{-22}
E. coli – water – BF 24 wk			-1.1×10^{-3}	9.8×10^{-22}
E. coli – water – BF 27 wk			-8.4×10^{-4}	7.8×10^{-22}

cells was captured on a membrane surface by filtering the cell suspension through a 0.45 μm membrane filter (Whatman 7184-004). The *E. coli* cell concentration on the filter was 10^8 cells/cm^2. This filter was kept on top of a 10% agar plate, containing 20% glycerol, to keep the cell lawn hydrated. The filters with *E. coli* lawn and the coupons from the CDC reactor were left undisturbed in a covered petri dish for 10–20 min before the contact angles measurements. This period of time was necessary to transfer the samples from the reactors and the media to the goniometer setup. The samples subjected to contact angle measurement were fully saturated with water and were not suitable for being probed with a water drop. Five microliters of diiodomethane was dropped on each surface, and contact angles were measured immediately for 10 s. Left and right contact angles for each surface in at least 3 locations were measured at least 12 times, with highest and lowest values discarded. The equilibrium contact angle was calculated as the average of each side contact angle.

All contact angle measurement was conducted after 30 min of air drying for biofilm. This protocol was similar one used in Park and Abu-Lail (2011) and has been confirmed by control experiments conducted with 24-week biofilms. See the Supplementary Material for details.

The Lifshitz–van der Waals (γ^{LW}) component of surface energy was derived from the contact angles using equation (4) in van Oss (1993). The LW component of free energy of adhesion (ΔG_{y0}^{LW}) between the *E. coli* and biofilm/PVC surface in the presence of water was calculated using Equation (2) in Liu et al. (2010). The Hamaker constant (*A*) was deduced from the LW component of free energy of adhesion (ΔG_{y0}^{LW}) as described in van Oss (1993).

2.4. Electrophoretic mobility

Electrophoretic mobilities (EM) of *E. coli* S17 and biofilm were measured by a Zetasizer Nano ZS90 instrument (Malvern Instruments, Southborough, MA) in various salt concentrations at 25 °C. An *E. coli* concentration of 3×10^6 *E. coli*/mL in each desired electrolyte solution buffered with 1 mM $NaHCO_3$ at pH 8.2–8.4 was used in electrophoretic mobility measurements. For biofilm, a PVC coupon from a CDC reactor was sonicated in 5 mL of a given salt concentration at pH 8.2–8.4 for 5 min. Six-week biofilms were sonicated for either 5 min or 30 min to assess the effect of sonication time on EM measurement. Supernatant was taken to measure EM. At least 3 replicates were conducted for each condition.

2.5. DLVO energy profiles

The total interaction energy between *E. coli* and a flat collector surface was calculated using the Hogg et al. (1966) expression. Electrostatic interaction (Φ_E) was calculated based on surface potentials, which was converted from electrophoretic mobilities via the Hemholtz-Smoluchowski equation. The van der Waals attractive interaction energy was calculated using the Gregory (1981) approximation. A Hamaker constant between *E. coli* and each surface is presented in Table 1.

2.6. Adhesion experiment

Adhesion of *E. coli* cells on biofilm and PVC surface was studied *ex-situ* in a PPFC (BioSurface Technologies Corp. FC 71). Adhesion experiments were performed at different

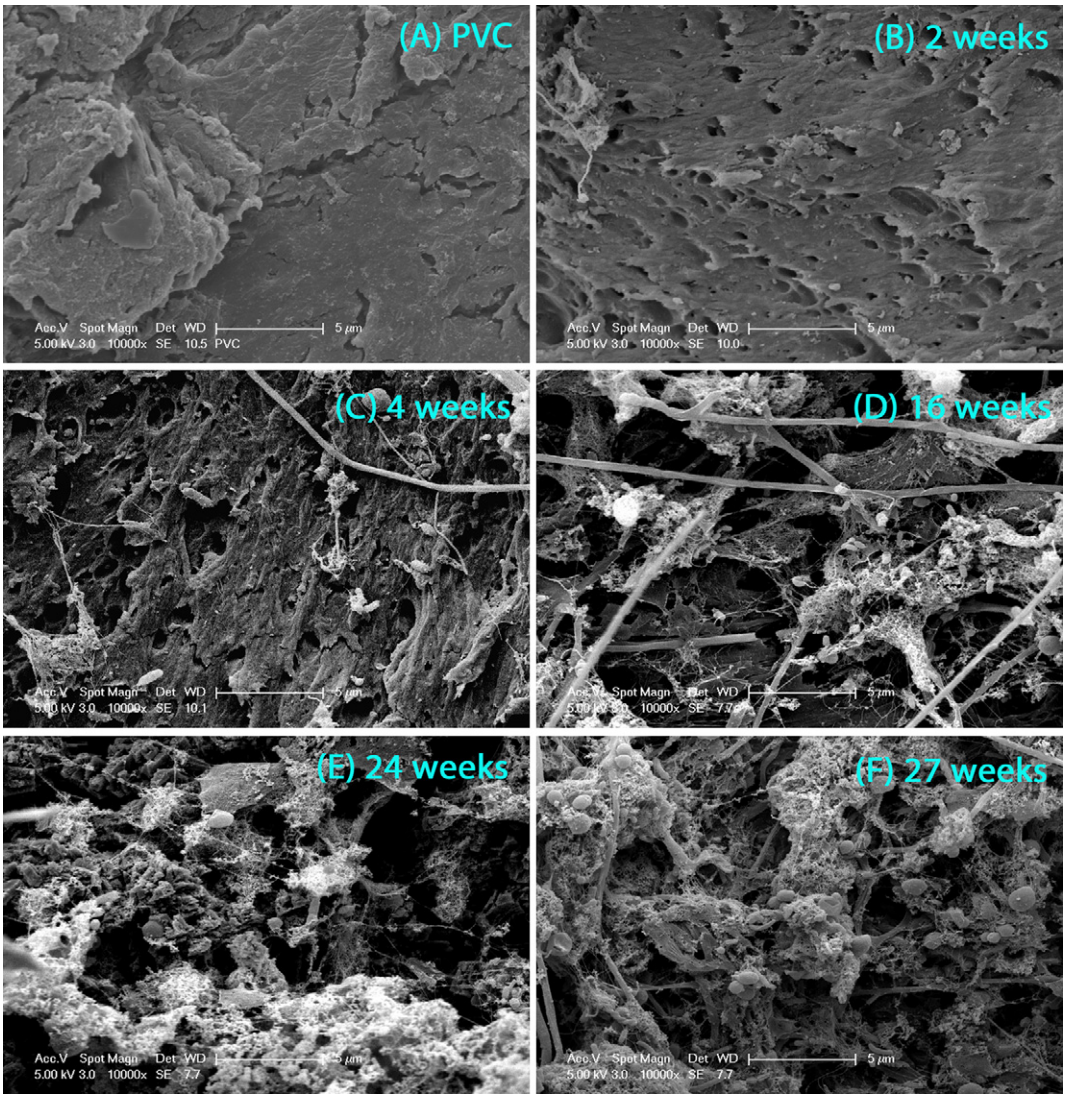

Fig. 1 – SEM images of (A) PVC, (B) 2-week old biofilm, (C) 4-week old biofilm, (D) 16-week old biofilm, (E) 24-week old biofilm, and (F) 27-week old biofilm at magnification of 10,000×. All biofilm samples were fixed, dried, and coated with Au before imaging.

monovalent concentrations (3–300 mM KCl) at 4×10^6 *E. coli* cells/mL with a constant flow of 1 ml/min. This chosen salt concentration is within the range of Urbana drinking water ionic strength (~3 mM, pH 8.3), as measured regularly using a conductivity probe. This range of ionic strength was used to determine the role of electrostatic interaction in *E. coli* adhesion to the biofilms. Electrolyte solutions were buffered at pH 8.2–8.4 by 1 mM sodium bicarbonate. The concentration of *E. coli* cells was selected to ensure that enough adhesion could be visualized, and no aggregation was observed during the adhesion experiment. Adhered *E. coli* cells were counted with a 40× objective in a rectangular viewing area of $296 \times 222\ \mu m^2$ under an inverted fluorescent microscope (Leica DM15000 M) every 15 s for 30 min. The microscope images were recorded by a QIMAGING RETIGA 2000R Fast 1394 camera and were processed by ImagePro 7.0 software. At the end of each experiment, the flow chamber was flushed with 1 mM KCl at the same flow rate for observation of possible cell detachment. Before the adhesion experiments, two control experiments were conducted. The first control experiment involved observing *E. coli* cells under a static no-flow condition on a glass slide using phase contrast and then fluorescence. The second control experiment involved observing *E. coli* cells under a continuous flow condition in a PPFC, for which glass coupons were used instead of biofilms so that the cells could be observed using a bright field and then fluorescence. The results of both control experiments confirmed that all *E. coli* cells were fluorescent and can be observed under both static and flow conditions.

2.7. *Flow profile for parallel flow chamber*

The parallel flow chamber used in our adhesion experiment had an inlet diameter of 1.45 mm (BioSurface Technologies

Corp. FC 71-PC-2 × 0.5). The width and the length of the flow channel were 13 mm and 39.3 mm, respectively. The depth of the flow cell was 0.39 mm. Inside the flow cell there were 2 slots to attach 2 PVC coupons; however, only 1 slot was used at a time in the adhesion experiment. The flow velocity profile was calculated by solving the Navier-Stokes equation using finite element algorithm in the software package COMSOL. The solution for the velocity profile was used to select a uniform laminar flow condition inside the parallel flow chamber. The adhesion was conducted at Re of 1.24, Pe of 0.3, and shear rate of 35 s^{-1}. Laminar flow condition was used in this study so that the role of solution chemistry and biofilm structure can be studied without additional influence of biofilm detachment and the change in biofilm structure due to shear.

2.8. Adhesion rate coefficient calculation and statistical analysis

The adhesion rate coefficient, k_d, was *E. coli* adhesion flux (number of deposited *E. coli* cells per viewing area per time) divided by initial *E. coli* cell concentration. Each condition was conducted twice within the same day with the same biofilms taken from the reactor to ensure consistency. Linear regression analysis was used to calculate the k_d value and the corresponding 95% confidence interval for data obtained for a given condition. k_d for each biofilm age was plotted as a function of ionic strength. A multiple linear regression analysis (Neter et al., 1990) was used to compare if the slopes of k_d versus ionic strength of each biofilm age were significantly different ($p < 0.05$) from each other. Only one k_d value was plotted in the graph. However, the adhesion experiment was conducted twice for each condition and they showed the same trend.

2.9. SEM sample preparation

All biofilm samples were fixed for SEM analysis using a method described previously (Clark et al., 2007). After fixation, biofilms were dried with a CO_2 critical point dryer (Tousimis, MD) and were sputter coated with gold-palladium. Biofilm samples were then viewed with a Philips XL30 field emission environmental scanning electron microscope (FEI, OR).

2.10. Collection of OCT biofilm images

OCT images of biofilm structures were captured in collaboration with the Biophotonics Imaging Laboratory at the Beckman Institute for Advanced Science and Technology (Nguyen et al., 2010; Xi et al., 2006). The Spectral-Domain OCT system for these studies utilized a mode-locked titanium:sapphire laser source (Kapteyn-Murnane Laboratories, Inc, Boulder, CO) centered at 800 nm with a bandwidth of 120 nm, providing an axial imaging resolution of 1.8 μm in water. The transverse resolution was 16 μm. The focus was set to be several centimeters beneath the glass surface of the sample holder where the biofilm structures were maintained. Two-dimensional cross-sectional images of 1 mm × 2 mm were acquired at an axial scan rate of 25 kHz, or at an approximate 40 ms acquisition time. The OCT system and OCT images are presented in the Supplemental materials.

The same version of the image analysis program that was used in Derlon et al. (2012) was used to analyze the OCT images. Image analysis consisted of the following steps:

(1) detecting the membrane–biofilm interface (grey-scale gradient analysis);
(2) binarizing the image (automatic thresholding);
(3) calculating the physical properties of the biofilm: mean biofilm thickness (in μm), absolute (R_a in μm) and relative roughness (R'_a) coefficients.

These parameters were calculated according to the following equations:

$$\bar{z} = \frac{1}{n}\sum_{i=1}^{N} z_i \tag{1}$$

$$R_a = \frac{1}{n}\sum_{i=1}^{N}\left(\left|z_i - \bar{z}\right|\right) \tag{2}$$

$$R'_a = \frac{1}{n}\sum_{i=1}^{N}\left(\frac{\left|z_i - \bar{z}\right|}{z}\right) \tag{3}$$

where N is the number of thickness measurements, is the local biofilm thickness (μm), and is the mean biofilm thickness (μm).

2.11. T-RFLP analysis of Biofilms

Biofilms grown from 2 to 25 weeks were collected for T-RFLP analysis (Liu et al., 1997). To collect the sample, PVC coupons were physically scraped with sterile cotton swabs. The cotton swabs were vortexed 3 times with the same buffer to retrieve the biomass as much as possible. The biomass-containing buffer solution was centrifuged at 12000× *g* and the pellets were kept at −80 °C before DNA extraction. Biofilm community DNA was extracted according to a protocol developed for drinking water biofilms (Hwang et al., 2012). The extracted DNA was air dried and re-dissolved in 50 μL milli-Q water. The amount of extracted DNA was measured with Nanodrop (Thermo Scientific, DE) and stored at −80 °C for further PCR analysis. T-RFLP was conducted as described previously (Liu et al. (1997) using a primer set 47F and 927R targeting the domain *Bacteria* 16S rRNA gene. The forward primer was labeled with 6-FAM. PCR reactions were conducted in a Bio-rad 1000 thermal cycler (Bio-rad, CA). Each reaction product was examined by gel electrophoresis with 1% agarose gel in TAE buffer at 100 V for 30 min. The final product was analyzed with ABI 3730 XL genetic analyzer at the Roy J. Carver Biotechnology Center at the University of Illinois. T-RFLP profiles were analyzed by Genemapper V 4.0. The peak binning was conducted with the Excel macro Treeflap (Rees et al., 2004). Statistical analysis was performed using PRIMER 6 software (Plymouth Marine Laboratory, UK). Relative abundance of terminal restrictive fragments (T-RFs) were tabulated, square-root transformed, and a distance matrix based on Bray–Curtis distance between samples was calculated. The similarities were visualized with cluster analysis.

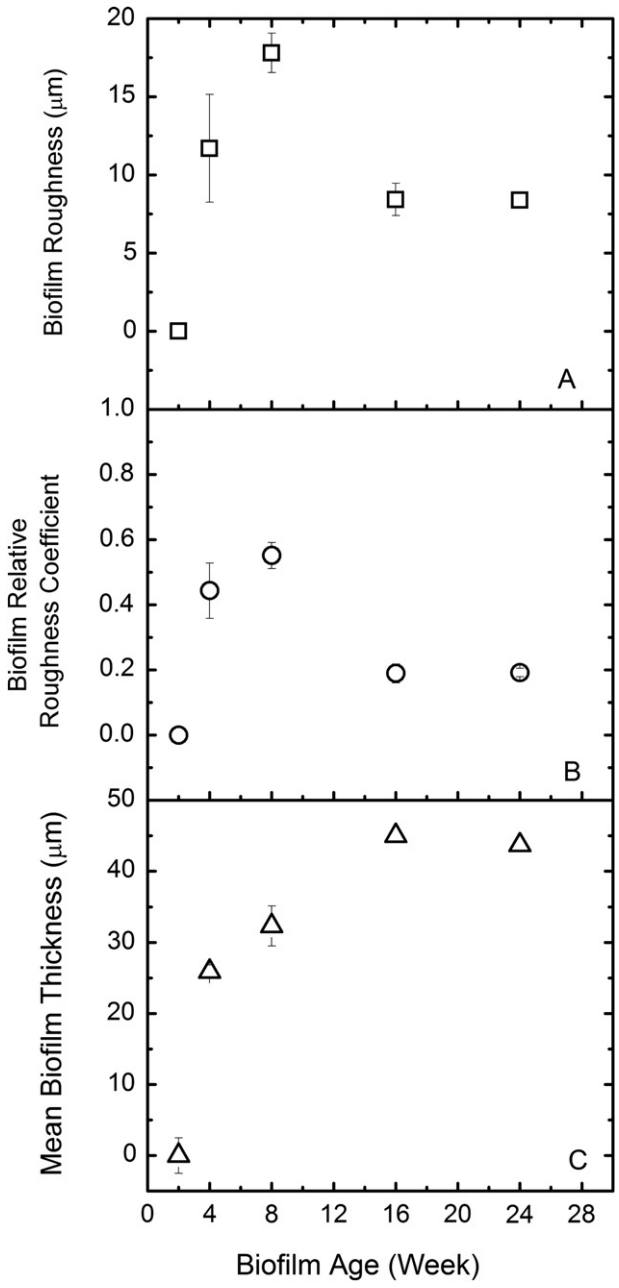

Fig. 2 – OCT biofilm characterization data calculated by using algorithm in Matlab. A) absolute biofilm roughness (μm), B) relative biofilm roughness coefficient, C) mean biofilm thickness (μm).

3. Results and discussion

3.1. Biofilm imaging and characterization

SEM and OCT imaging techniques were selected to characterize the physical properties of the biofilms at microscopic and mesoscopic resolution, respectively. SEM images (Fig. 1) showed that after 2 weeks of feeding with groundwater, only a small fraction of the PVC coupons in the CDC reactor was covered by biofilm, and after 4 weeks the entire surface of the coupons was covered with mainly extracellular polymeric substances (EPS). The 2-week old biofilm was too thin to allow quantitative analysis of roughness with OCT. For 4-week and up to 24-week old biofilms, the changes in the biofilm roughness (Fig. 2A) and mean thickness (Fig. 2B) were monitored. The biofilm roughness increased from 11.7 ± 3.5 μm to 17 ± 1.3 μm until week 16, and then decreased to 8 ± 0.5 μm between week 16 and 24 (Fig. 2A). At week 16, the mean biofilm thickness increased to 45 ± 4 μm. At week 24, a stable mean biofilm thickness of 44 ± 1.5 μm was obtained (Fig. 2C). Based on the thickness, roughness, and coverage data (qualitatively) determined by OCT and SEM, the biofilms seemed to be physically stable after 16 weeks. Both conventional and reflectance CSLM techniques were also applied for these biofilms. However, the thickness, the unknown composition of the biofilms, and the complicated structure of the thick biofilms did not allow images with sufficient quality for quantitative analysis. These issues have been reported in previous studies on biofilm structures (Vroom et al., 1999; Wood et al., 2002).

3.2. Biofilm community analysis

Biological stability of the groundwater biofilms was determined by analyzing microbial community diversity with T-RFLP for biofilms ranging from 2 weeks to 25 weeks. The resulting electrophoregrams indicated that there was a shift in the major terminal restriction fragments (T-RFs). For the 2-week old biofilms, the 106-bp T-RF was detected to account for 75.9% of the total peak area (Fig. 4S-1). The abundance of the same fragment was reduced to 24.5% for the 6-week old biofilms (Fig. 4S-2). For biofilm samples after eight weeks (Fig. 4S-3–7), major T-RFs were shifted to 88 bp and 400 bp, suggesting that a microbial succession was taking place during the CDC operation. The change in the most abundant T-RF suggests a change in the dominant groups of microbial communities during the biofilm development. During the entire experiment, T-RFs with fragment lengths of 83 bp, 95 bp, and 363 bp were observed in all biofilm samples.

The T-RFLP fingerprinting profiles were used to calculate the similarity index between samples, and to construct cluster analysis and determine the relative similarities among the communities. The cluster analysis results (Fig. 3) showed two separate clusters for “young” biofilms between 2 weeks and 6 weeks, and “old” biofilms longer than 14 weeks. This observation agreed with the physical characterization results based on SEM and OCT measurements. Among all biofilm samples, the highest similarity was observed among samples taken at 18, 20, and 25 weeks, suggesting that a stable microbial community was formed in biofilms at the late phase of the experiment.

For biofilm samples taken between weeks 2 and 8, increasing thickness and roughness were observed together with a change in the microbial community structure of those young biofilms. This observation was in agreement with the incomplete coverage of the PVC coupons by 2-week old biofilm shown in the SEM image (Fig. 1). For 8-week and 14/16-week old biofilms, increasing thickness and decreasing roughness were correlated with unstable community structure as shown by cluster analysis. The observation that the biofilm

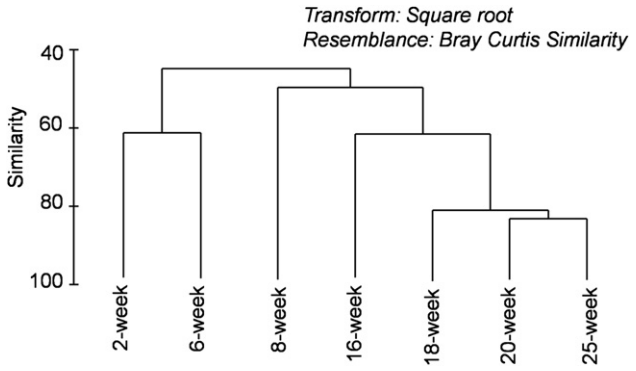

Fig. 3 – Cluster analysis of T-RFLP for biofilm community diversity.

community became stabilized between weeks 18 and 25 was consistent with similar thickness and roughness observed for 16-week and 24-week old biofilms. The SEM images for 16-, 24-, and 27-week old biofilms also showed that the PVC coupons were completely covered with biofilms. In summary, both physical and biological biofilm characteristics suggest that the development of biofilms was mostly taking place from week zero to 16 weeks, and reached stable biofilm structure after 18 weeks of feeding. The general classification between young and old biofilms was further used to explain adhesion of *E. coli* cells and CML particles on biofilms.

3.3. *Electrophoretic mobility*

Fig. 4 shows the electrophoretic mobility of biofilms obtained at different growth periods. Less negative electrophoretic mobility was observed with increasing ionic strength. However, at a given ionic strength, comparable values for electrophoretic mobility of biofilms taken at weeks 2, 6, and 8 were observed. Specifically, electrophoretic mobility at 3 mM KCl was -1.5 ± 0.08 μmV s^{-1} cm^{-1} and -1.4 ± 0.12 μmV s^{-1} cm^{-1} for 2- and 6-week old biofilms, respectively. At 10 mM ionic strength, the 4- and 27-week old biofilms showed slightly more negatively charged electrophoretic mobility than the 2-, 6-, and 8-week old biofilms. However, at 300 mM, all biofilms had statistically similar electrophoretic mobility. For 6-week old biofilms, electrophoretic mobilities measured in 10 mM and 300 mM ionic strength solutions were similar for samples sonicated for 5 min or 30 min. Specifically, electrophoretic mobilities of 6-week biofilms were -1.4 ± 0.12 μmV S^{-1} cm^{-1} and -1.5 ± 0.15 μmV S^{-1} cm^{-1} for 5 and 30 min sonication. Apparently, the duration of sonication did not have influence on the EM result, as it showed no difference in zeta potential at different sonication times. However, sonication of biofilms was likely to remove the entire biofilm from the PVC coupons, and the electrophoretic measurement represented the whole biofilm, not just the biofilm surface. The electrophoretic mobility and the corresponding zeta potential of *E. coli* cells in the presence of KCl are presented in Fig. 4. All measurements were measured at 25 °C and at pH 8.2–8.5 for ionic strengths ranging from 3 to 300 mM KCl.

The EM of *E. coli* cells were -3.3 ± 0.1 μmV s^{-1} cm^{-1} and -0.5 ± 0.2 μmV s^{-1} cm^{-1} at 3 mM and 600 mM, respectively. The observed EM for *E. coli* cells were more negative than those of other *E. coli* strains reported by Walker et al. (2005) because of higher pH (8.2–8.5) used in this current work. The electrophoretic mobility of *E. coli* has been reported to become more negative with increasing pH (Kim et al., 2009). Compared to *E. coli* cells, CML particles were more negatively charged (Fig. 4). Under all experimental conditions, the electrophoretic mobility of *E. coli* cells, biofilms, and CML particles were negative, and became less negative with increasing ionic strength. This observation suggests that double layer compression led to lower surface charge, and electrostatics interactions may control adhesion of *E. coli* cells and CML particles to these biofilms. If this is the case, higher electrostatic repulsion was expected for CML adhesion on biofilm compared to *E. coli* adhesion on the same biofilm.

3.4. *Contact angle of* E. coli *cells and other substrates*

The van der Waal interaction between the biofilms and *E. coli* cells or CML particles is determined by the Hamaker's constant (A). The constants for *E. coli*-biofilm-water and CML-biofilm-water were calculated from the contact angles of diiodomethane on *E. coli* cells, CML, PVC, and biofilms at different ages. As shown in Table 1, the contact angle of non-polar hydrophobic diiodomethane on *E. coli* cells (70.6°±2.2°) was the most polar and hydrophilic followed by CML (55.1°±2°), PVC (49.8°±2.2°), and biofilms (26°–43°). With increasing biofilm age, the contact angle became smaller, which suggested a less polar surface and more hydrophobic biofilm surface.

Lifshitz–van der Waals components of free energy of adhesion (ΔG_{y0}^{LW}) between *E. coli* and CML and the collector surfaces are listed in Table 1 ΔG_{y0}^{LW} was less negative with increasing biofilm ages. As a result of less negative values of ΔG_{y0}^{LW} for older biofilms, the Hamaker's constant (A) was calculated based on Lifshitz–van der Waals components of free energy of adhesion (ΔG_{y0}^{LW}) between *E. coli* or CML and each surface became smaller (Table 1). The Hamaker's constant of *E. coli* – water – PVC (1.5×10^{-21} J) measured here is comparable to the Hamaker's constant of *E. coli* – water – quartz used in the literature (6.5×10^{-21} J) (Walker et al., 2005, 2004, 2006; Redman et al., 2004), and *cryptosporidium* oocyst – water – quartz (6.5×10^{-21} J) (Liu et al., 2010).

3.5. *Total energy barrier between* E. coli *and a biofilm*

The zeta potential and Hamaker constants determined above were used to calculate the energy barrier between biofilms and *E. coli* cells or CML particles according to the Derjaguin, Landau, Verwey and Overbeek (DLVO) theory (Table 2). As shown above, similar values of zeta potential for biofilms grown at different lengths of time (Fig. 4) suggested that the repulsive interaction between *E. coli* cells and the biofilms is similar for these biofilms. The values of Hamaker's constant (A) determined from the contact angle measurement were used to calculate the van der Waals energy interaction components for the DLVO energy profiles. Smaller Hamaker's constants (Table 1) indicated weaker van der Waals interaction for older biofilms. However, the small difference in van der Waals interaction was overwhelmed by repulsion

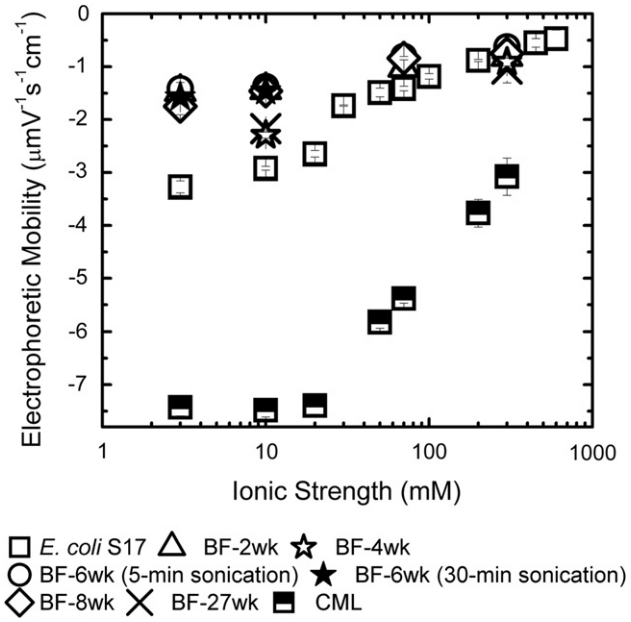

Fig. 4 – Electric surface charge properties of *E. coli* S17 (square), 2-week old biofilm (triangle), 4-week old biofilm (open star), 6-week old biofilm with 5-min sonication (open circle), 6-week biofilm with 30-min sonication (closed star), 8-week old biofilm (diamond), 27-week old biofilm (cross) as a function of ionic strength (KCl) at pH 8.2–8.5. Zeta potential was calculated from experimental electrophoretic mobility using Smoluchowski equation.

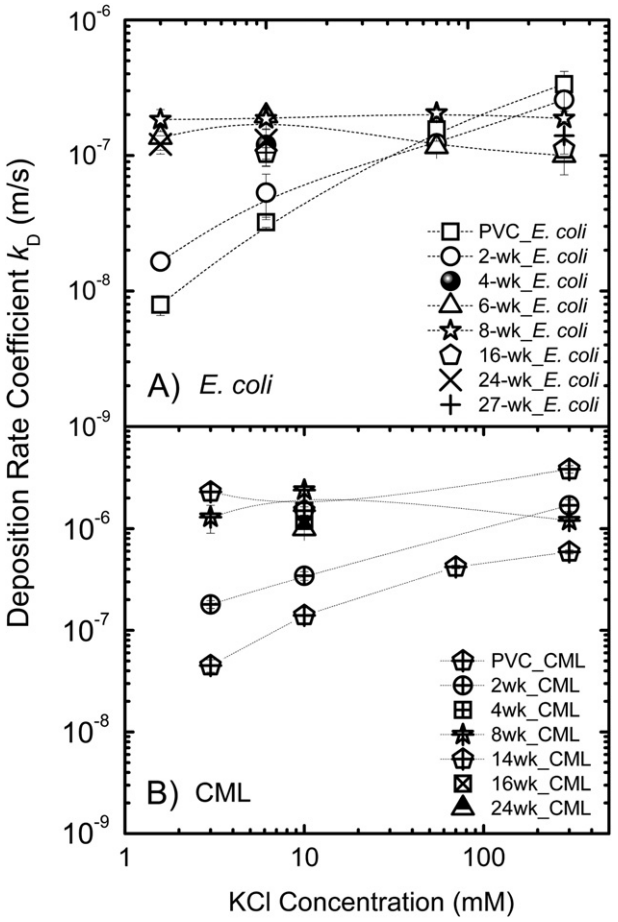

Fig. 5 – Adhesion rate coefficient (k_a) of A) *E. coli* S17, and B) CML on clean PVC and biofilm surface grown at different times as a function of ionic strength (KCl) at pH 8.2–8.5 and at 25 °C. The error bars correspond to 95% confidence intervals.

interaction. As a result, energy barriers were present for 3, 10, and 70 mM (Table 2). For example, interaction energies of 2- and 8-week old biofilms in 10 mM were 308 and 313 kT, respectively. For 27-week old biofilms in 10 mM, the interaction energy was 601 kT, which was higher than interaction energies of 2- and 8-week old biofilms due to the more negative electrophoretic mobility. Interaction energies between CML and different ages of biofilms at 10 mM KCl also showed the same trend as *E. coli* cells. For example, the interaction energies of 2- and 8-week old biofilms in 10 mM were 357 and 367 kT, respectively. For 27-week old biofilms in 10 mM, the interaction energy was 798 kT. These high interaction energies suggest low or no adhesion of *E. coli* cells or CML particles on biofilms. Moreover, the fact that interaction energies are present at every ionic strength suggests that low adhesion rates of *E. coli* cells or CML particles should be observed.

As predicted by the DLVO theory, energy barriers decreased with ionic strength. Specifically, on 2-week old biofilms, interaction energies at 3 and 300 mM were 342 and 0 kT, respectively. On 27-week old biofilms, interaction energies at 10 and 300 mM, which were 601 and 0.5 kT, respectively, decreased with ionic strength. However, the presence of energy barriers were observed even at high ionic strength, suggesting that adhesion of *E. coli* cells on biofilms should be unfavorable.

Table 2 – A) Interaction energy between *E. coli* and biofilms at different age and ionic strength, and B) interaction energy between CML and biofilms at different age and ionic strength.

Interaction energy (kT)				
IS (mM)	2 week	6 week	8 week	27 week
A) *E. coli*				
3	342	315	463	–
10	308	284	313	601
70	75	45	50	–
300	0	0	0	0.5
B) CML				
3	374	345	523	–
10	357	326	367	798
70	171	112	120	–
300	105	65	93	179

3.6. *Adhesion kinetics of* E. coli *cells and CML particles*

The adhesion kinetics data for *E. coli* cells and CML particles on biofilms and PVC coupons were obtained and compared with the trends predicted by the DLVO theory. Adhesion rate

coefficients of *E. coli* cells on PVC surface and 2-week old biofilm were observed to increase with ionic strength (Fig. 5). Specifically, k_d of *E. coli* cells on PVC increased from $(7.9 \pm 1.3) \times 10^{-9}$ to $(3.4 \pm 0.8) \times 10^{-7}$ m/s at 3 and 300 mM, respectively. The same trend was observed for CML particles. The k_d of CML on PVC increased from $(4.5 \pm 0.6) \times 10^{-8}$ to $(5.9 \pm 0.3) \times 10^{-7}$ m/s at 3 and 300 mM, respectively. On 2-week old biofilms, k_d of *E. coli* cells and CML particles showed the increasing trend from low to high ionic strength as well. As observed by SEM, 2-week old biofilms were not yet fully established on PVC surface, and *E. coli* cells or CML particles were likely to deposit on both the biofilm surface and uncovered PVC surface. The increase in adhesion rates with solution ionic strength could be expected based on DLVO theory because less negative surface charge of *E. coli* cells, CML, and biofilm in higher ionic strength solutions due to the compression of double layer thickness could lead to higher adhesion. Thus, for PVC and 2-week old biofilms, electrostatic interaction played an important role in controlling both *E. coli* cells and CML particle adhesion.

The adhesion rate coefficients of *E. coli* cells measured at ionic strengths from 3 mM to 300 mM were statistically the same ($p < 0.05$) on biofilm from week 6 and older. Specifically, k_d of *E. coli* cells on 6-week old biofilm were $(1.3 \pm 0.3) \times 10^{-7}$ and $(1.0 \pm 0.1) \times 10^{-7}$ m/s at 3 and 300 mM, respectively. On the biofilms at 27 weeks, the adhesion rate coefficients of *E. coli* cells were $(1.0 \pm 0.1) \times 10^{-7}$ and $(1.4 \pm 0.4) \times 10^{-7}$ m/s at 10 and 300 mM, respectively. Adhesion rate coefficients of CML particles on 8-week old biofilms were also found to be independent of ionic strength. Specifically, k_d of CML on 8-week old biofilms were $(1.3 \pm 0.4) \times 10^{-6}$ and $(1.2 \pm 0.4) \times 10^{-6}$ m/s at 3 and 300 mM, respectively. The observation that adhesion was independent of ionic strength for both *E. coli* cells and CML particles qualitatively disagreed with lower energy barriers calculated from DLVO theory for these biofilms (Table 2). It is likely that the adhesion of *E. coli* cells or CML particles on 8-week and older biofilms was not mainly controlled by classic DLVO forces such as electrostatic and van der Waals interactions. The surface structure of biofilms such as thickness and roughness was further investigated.

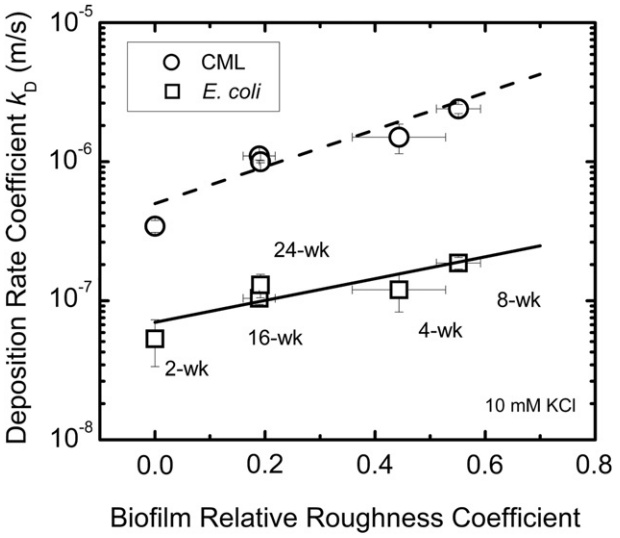

Fig. 6 – Adhesion rate coefficient (k_d) of *E. coli* S17 as a function of biofilm relative roughness coefficient at different biofilm ages. Adhesion experiments were carried out at 10 mM KCl, pH 8.2–8.5 at room temperature. For 2-week old biofilm, the biofilm roughness coefficients were undetected because the biofilms were too thin for OCT imaging.

Adhesion rate coefficients of biofilms were found to increase with biofilm relative roughness (Fig. 6). Specifically, adhesion rate coefficients of *E. coli* cells increased from $(1.0 \pm 0.1) \times 10^{-7}$ to $(1.9 \pm 0.2) \times 10^{-7}$ m/s for 16- and 8- week old biofilms, while biofilm roughness coefficients changed from 0.2 ± 0.03 to 0.55 ± 0.04. In addition, adhesion rate coefficients of *E. coli* cells on biofilms at weeks 16 and 24 were similar ($(1.0 \pm 0.1) \times 10^{-7}$ m/s and $(1.3 \pm 0.3) \times 10^{-7}$ m/s, respectively), and so were the biofilm surface roughness coefficients (0.2 ± 0.03 to 0.2 ± 0.01, respectively). The physical biofilm structure in terms of relative roughness also influenced the CML adhesion (Fig. 6). Adhesion rate coefficients of CML increased from $(1.1 \pm 0.07) \times 10^{-6}$ m/s to $(2.4 \pm 0.2) \times 10^{-6}$ m/s for 16- and 8- week old biofilms, respectively. The adhesion rate coefficients of CML were also similar for 16- and 24-week old biofilms ($(1.1 \pm 0.07) \times 10^{-6}$ m/s and $(1.0 \pm 0.02) \times 10^{-6}$ m/s, respectively).

Our observation that both *E. coli* and CML particles had higher adhesion on biofilms with higher roughness is consistent with previous work on oocysts and *E. coli* adhesion to *P. aeruginosa* biofilms (Searcy et al., 2006; Wu et al., 2012), and on oocyst adhesion to biofilms collected from rivers (DiCesare et al., 2012). Roughness was also found to influence adhesion of colloidal particles to abiotic surfaces (Chen et al., 2010; Subramani and Hoek, 2010). An extended DLVO theory has been developed to explain enhanced attachment of particles on rough surfaces. According to this model, for like-charged surfaces, the energy barrier estimated between the colloids and the polymeric membrane surface with semispherical asperities was lower compared to that between the colloids and the smooth membrane surface to allow more deposition on rough surface compared to deposition on smooth surface (Hoek and Agarwal, 2006; Hoek et al., 2003; Huang et al., 2010).

As discussed above, lower Hamaker constant and more negative zeta potential for CML compared to *E. coli* cells suggested that the energy barrier between CML and the glass surface should be higher than that between *E. coli* cells and the glass surface (747 kT for CML vs. 580 kT for *E. coli*). Higher energy barrier should lead to lower adhesion. In contrast to our expectation, the adhesion of CML is 10 times higher than *E. coli* at all biofilm ages and ionic strengths (Fig. 5). Specifically, k_d of CML and *E. coli* on 2-week old biofilm is $(1.8 \pm 0.1) \times 10^{-7}$ and $(1.6 \pm 0.2) \times 10^{-8}$, respectively. In addition to adhesion on PVC coupons, an additional set of *E. coli* cells and CML adhesion on clean glass surface in 10 mM ionic strength solution was conducted. A similar trend for the 2-week old biofilm was observed; k_d of CML and *E. coli* on the glass surface was $(1.6 \pm 0.2) \times 10^{-6}$ and $(4.8 \pm 0.7) \times 10^{-9}$. In addition to DLVO interactions that control *E. coli* adhesion on the glass surface, steric repulsion due to the presence of macromolecules on the *E. coli* cell surface may lower *E. coli* adhesion compared to the adhesion of CML particles. This steric interaction has previously been found for bacteria and oocyst deposition (Liu et al., 2010; Rijnaarts et al., 1999).

To test the effect of water hardness on *E. coli* cell adhesion on biofilms, the adhesion experiment of *E. coli* in Newmark groundwater was conducted on the 24-week old biofilms in the presence of filtered groundwater. The adhesion rate coefficients were statistically the same ($p < 0.05$) for groundwater and solutions containing 3 or 10 mM KCl ($(1.2 \pm 0.2) \times 10^{-7}$ for 3 mM, $(1.3 \pm 0.3) \times 10^{-7}$ for 10 mM, and $(1.6 \pm 0.6) \times 10^{-7}$ m/s for groundwater). Newmark groundwater (pH 7.8) had an alkalinity of 330 mg/L as $CaCO_3$, and contained 1.5 mM Ca^{2+} and 1.0 mM Mg^{2+}. The similarity of *E. coli* adhesion in solution with and without hardness suggested that typical hardness of drinking water did not influence *E. coli* adhesion.

4. Conclusions

- The mechanisms of *E. coli* attachment change depending on the age of the biofilms.
- The physico-chemical properties of the water (ionic strength, hardness) govern the adhesion rate of *E.coli* cells and CML particles on PVC surfaces and on young/thin biofilms (age <8 weeks). An increasing ionic strength/hardness increases the adhesion rates.
- The physical biofilm properties govern *E.coli* cell attachment in the case of mature biofilms (age >16 weeks). An increasing biofilm roughness increases the adhesion rate. Because the biofilm in DWDS is likely to be mature biofilm, subsequent study should focus on pathogen cells entrapped in the pores of the biofilm.

Acknowledgment

This publication was made possible by USEPA grant R834870. Its contents are solely the responsibility of the grantee and do not necessarily represent the official views of the USEPA. Further, USEPA does not endorse the purchase of any commercial products or services mentioned in the publication. DJ is supported by the Royal Thai Scholarship. Yun Shen is acknowledged in helping to collect the CML data.

Appendix A. Supplementary data

Supplementary data related to this article can be found at http://dx.doi.org/10.1016/j.watres.2013.02.032.

REFERENCES

Altman, S.J., McGrath, L.K., Souza, C.A., Murton, J.K., Camper, A.K., 2009. Integration and decontamination of *Bacillus cereus* in *Pseudomonas fluorescens* biofilms. Journal of Applied Microbiology 107 (1), 287–299.

Berry, D., Xi, C., Raskin, L., 2006. Microbial ecology of drinking water distribution systems. Current Opinion in Biotechnology 17 (3), 297–302.

Berry, D., Xi, C.W., Raskin, L., 2009. Effect of growth conditions on inactivation of *Escherichia coli* with monochloramine. Environmental Science & Technology 43 (3), 884–889.

Bradley, I., Straub, A., Maraccini, P., Markazi, S., Nguyen, T.H., 2011. Iron oxide amended biosand filters for virus removal. Water Research 45 (15), 4501–4510.

Brant, J.A., Childress, A.E., 2002. Assessing short-range membrane–colloid interactions using surface energetics. Journal of Membrane Science 203 (1–2), 257–273.

Busscher, H.J., Weerkamp, A.H., Vandermei, H.C., Vanpelt, A.W.J., Dejong, H.P., Arends, J., 1984. Measurement of the surface free energy of bacteria cell surfaces and its relevance for adhesion. Applied and Environmental Microbiology 48 (5), 980–983.

Chen, G.X., Bedi, R.S., Yan, Y.S., Walker, S.L., 2010. Initial colloid deposition on bare and zeolite-coated stainless steel and aluminum: influence of surface roughness. Langmuir 26 (15), 12605–12613.

Clark, M.E., Edelmann, R.E., Duley, M.L., Wall, J.D., Fields, M.W., 2007. Biofilm formation in *Desulfovibrio vulgaris* Hildenborough is dependent upon protein filaments. Environmental Microbiology 9 (11), 2844–2854.

Craun, G.F., Hubbs, S.A., Frost, F., Calderon, R.L., Via, S.H., 1998. Waterborne outbreaks of cryptosporidiosis. Journal American Water Works Association 90 (9), 81–91.

Craun, G.F., Nwachuku, N., Calderon, R.L., Craun, M.F., 2002. Outbreaks in drinking-water systems, 1991–1998. Journal of Environmental Health 65 (1), 16–23.

Craun, G.F., Brunkard, J.M., Yoder, J.S., Roberts, V.A., Carpenter, J., Wade, T., Calderon, R.L., Roberts, J.M., Beach, M.J., Roy, S.L., 2010. Causes of outbreaks associated with drinking water in the United States from 1971 to 2006. Clinical Microbiology Reviews 23 (3), 507–528.

Declerck, P., Behets, J., Margineanu, A., van Hoef, V., De Keersmaecker, B., Ollevier, F., 2009. Replication of *Legionella pneumophila* in biofilms of water distribution pipes. Microbiological Research 164 (6), 593–603.

Derlon, N., Peter-Varbanets, M., Scheidegger, A., Pronk, W., Morgenroth, E., 2012. Predation influences the structure of biofilm developed on ultrafiltration membranes. Water Research 46 (10), 3323–3333.

DiCesare, E.A.W., Hargreaves, B.R., Jellison, K.L., 2012. Biofilm roughness determines *Cryptosporidium parvum* retention in environmental biofilms. Applied and Environmental Microbiology 78 (12), 4187–4193.

Falkinham, J.O., Norton, C.D., LeChevallier, M.W., 2001. Factors influencing numbers of *Mycobacterium avium, Mycobacterium intracellulare*, and other mycobacteria in drinking water distribution systems. Applied and Environmental Microbiology 67 (3), 1225–1231.

Flemming, H.C., Wingender, J., 2010. The biofilm matrix. Nature Reviews Microbiology 8 (9), 623–633.

Gagnon, G.A., Baribeau, H., Rutledge, S.O., Dumancic, R., Oehmen, A., Chauret, C., Andrews, S., 2008. Disinfectant efficacy in distribution systems: a pilot-scale assessment. Journal of Water Supply Research and Technology-Aqua 57 (7), 507–518.

Gregory, J., 1981. Approximate expressions for retarded van der waals interaction. Journal of Colloid and Interface Science 83 (1), 138–145.

Haisch, C., Niessner, R., 2007. Visualisation of transient processes in biofilms by optical coherence tomography. Water Research 41 (11), 2467–2472.

Helmi, K., Skraber, S., Gantzer, C., Willame, R., Hoffmann, L., Cauchie, H.M., 2008. Interactions of *Cryptosporidium parvum, Giardia lamblia*, vaccinal poliovirus type 1, and bacteriophages phi X174 and MS2 with a drinking water biofilm and a wastewater biofilm. Applied and Environmental Microbiology 74 (7), 2079–2088.

Helmi, K., Menard-Szczebara, F., Lenes, D., Jacob, P., Jossent, J., Barbot, C., Delabre, K., Arnal, C., 2010. Adenovirus, MS2 and PhiX174 interactions with drinking water biofilms developed

on PVC, cement and cast iron. Water Science and Technology 61 (12), 3198–3207.
Hoek, E.M.V., Agarwal, G.K., 2006. Extended DLVO interactions between spherical particles and rough surfaces. Journal of Colloid and Interface Science 298 (1), 50–58.
Hoek, E.M.V., Bhattacharjee, S., Elimelech, M., 2003. Effect of membrane surface roughness on colloid-membrane DLVO interactions. Langmuir 19 (11), 4836–4847.
Hogg, R., Healy, T.W., Fuerstenau, D.W., 1966. Mutual coagulation of colloidal dispersions. Transactions of the Faraday Society 62, 1638–1651.
Huang, X., Bhattacharjee, S., Hoek, E.M.V., 2010. Is surface roughness a "Scapegoat" or a primary factor when defining particle-substrate interactions? Langmuir 26 (4), 2528–2537.
Hwang, C.C., Ling, F.Q., Andersen, G.L., LeChevallier, M.W., Liu, W.T., 2012. Evaluation of methods for the extraction of DNA from drinking water distribution system biofilms. Microbes and Environments 27 (1), 9–18.
Karunakaran, E., Mukherjee, J., Ramalingam, B., Biggs, C.A., 2011. "Biofilmology": a multidisciplinary review of the study of microbial biofilms. Applied Microbiology and Biotechnology 90 (6), 1869–1881.
Kim, H.N., Hong, Y., Lee, I., Bradford, S.A., Walker, S.L., 2009. Surface characteristics and adhesion behavior of *Escherichia coli* O157:H7: role of extracellular macromolecules. Biomacromolecules 10 (9), 2556–2564.
Kumar, C.G., Anand, S.K., 1998. Significance of microbial biofilms in food industry: a review. International Journal of Food Microbiology 42 (1–2), 9–27.
Långmark, J., Storey, M.V., Ashbolt, N.J., Stenström, T.-A., 2005. Accumulation and fate of microorganisms and microspheres in biofilms formed in a pilot-scale water distribution system. Applied and Environmental Microbiology 71 (2), 706–712.
Lau, H.Y., Ashbolt, N.J., 2009. The role of biofilms and protozoa in *Legionella* pathogenesis: implications for drinking water. Journal of Applied Microbiology 107 (2), 368–378.
Le Dantec, C., Duguet, J.P., Montiel, A., Dumoutier, N., Dubrou, S., Vincent, V., 2002. Occurrence of mycobacteria in water treatment lines and in water distribution systems. Applied and Environmental Microbiology 68 (11), 5318–5325.
Li, Q.L., Snoeyink, V.L., Campos, C., Marinas, B.J., 2002. Displacement effect of NOM on atrazine adsorption by PACs with different pore size distributions. Environmental Science & Technology 36 (7), 1510–1515.
Liu, W.T., Marsh, T.L., Cheng, H., Forney, L.J., 1997. Characterization of microbial diversity by determining terminal restriction fragment length polymorphisms of genes encoding 16S rRNA. Applied and Environmental Microbiology 63 (11), 4516–4522.
Liu, Y., Kuhlenschmidt, M.S., Kuhlenschmid, T.B., Nguyen, T.H., 2010. Composition and conformation of *Cryptosporidium parvum* oocyst wall surface macromolecules and their effect on adhesion kinetics of oocysts on quartz surface. Biomacromolecules 11 (8), 2109–2115.
Neter, J., Wasserman, W., Kutner, M.H., 1990. Applied Linear Statistical Models: Regression, Analysis of Variance, and Experimental Designs. Irwin, Homewood, IL.
Nguyen, C.T., Tu, H.H., Chaney, E.J., Stewart, C.N., Boppart, S.A., 2010. Non-invasive optical interferometry for the assessment of biofilm growth in the middle ear. Biomedical Optics Express 1 (4), 1104–1116.
Nguyen, C.T., Jung, W., Kim, J., Chaney, E.J., Novak, M., Stewart, C.N., Boppart, S.A., 2012. Noninvasive in vivo optical detection of biofilm in the human middle ear. Proceedings of the National Academy of Sciences of the United States of America 109 (24), 9529–9534.
Norton, C.D., LeChevallier, M.W., Falkinham, J.O., 2004. Survival of *Mycobacterium avium* in a model distribution system. Water Research 38 (6), 1457–1466.
Paris, T., Skali-Lami, S., Block, J.-C., 2007. Effect of wall shear rate on biofilm deposition and grazing in drinking water flow chambers. Biotechnology and Bioengineering 97 (6), 1550–1561.
Paris, T., Skali-Lami, S., Block, J.-C., 2009. Probing young drinking water biofilms with hard and soft particles. Water Research 43 (1), 117–126.
Park, B.-J., Abu-Lail, N.I., 2011. The role of the pH conditions of growth on the bioadhesion of individual and lawns of pathogenic *Listeria* monocytogenes cells. Journal of Colloid and Interface Science 358 (2), 611–620.
Redman, J.A., Walker, S.L., Elimelech, M., 2004. Bacterial adhesion and transport in porous media: role of the secondary energy minimum. Environmental Science & Technology 38 (6), 1777–1785.
Rees, G.N., Baldwin, D.S., Watson, G.O., Perryman, S., Nielsen, D.L., 2004. Ordination and significance testing of microbial community composition derived from terminal restriction fragment length polymorphisms: application of multivariate statistics. Antonie Van Leeuwenhoek International Journal of General and Molecular Microbiology 86 (4), 339–347.
Rijnaarts, H.H.M., Norde, W., Lyklema, J., Zehnder, A.J.B., 1999. DLVO and steric contributions to bacterial deposition in media of different ionic strengths. Colloids and Surfaces B-biointerfaces 14 (1–4), 179–195.
Searcy, K.E., Packman, A.I., Atwill, E.R., Harter, T., 2006. Capture and retention of *Cryptosporidium parvum* oocysts by *Pseudomonas aeruginosa* biofilms. Applied and Environmental Microbiology 72 (9), 6242–6247.
Simon, R., Priefer, U., Puhler, A., 1983. A broad host range mobilization system for in vivo genetic engineering: transposon mutagenesis in gram negative bacteria. Bio/Technology 1 (9), 784–791.
Subramani, A., Hoek, E.M.V., 2010. Biofilm formation, cleaning, re-formation on polyamide composite membranes. Desalination 257 (1–3), 73–79.
Torvinen, E., Suomalainen, S., Lehtola, M.J., Miettinen, I.T., Zacheus, O., Paulin, L., Katila, M.L., Martikainen, P.J., 2004. *Mycobacteria* in water and loose deposits of drinking water distribution systems in Finland. Applied and Environmental Microbiology 70 (4), 1973–1981.
Valster, R.M., Wullings, B.A., van den Berg, R., van der Kooij, D., 2011. Relationships between free-living protozoa, cultivable *Legionella* spp., and water quality characteristics in three drinking water supplies in the Caribbean. Applied and Environmental Microbiology 77 (20), 7321–7328.
van der Mei, H.C., Bos, R., Busscher, H.J., 1998. A reference guide to microbial cell surface hydrophobicity based on contact angles. Colloids and Surfaces B-Biointerfaces 11 (4), 213–221.
van Oss, C.J., 1993. Acid – base interfacial interactions in aqueous media. Colloids and Surfaces A: Physicochemical and Engineering Aspects 78 (0), 1–49.
Vroom, J.M., De Grauw, K.J., Gerritsen, H.C., Bradshaw, D.J., Marsh, P.D., Watson, G.K., Birmingham, J.J., Allison, C., 1999. Depth penetration and detection of pH gradients in biofilms by two-photon excitation microscopy. Applied and Environmental Microbiology 65 (8), 3502–3511.
Walker, S.L., Redman, J.A., Elimelech, M., 2004. Role of cell surface lipopolysaccharides in *Escherichia coli* K12 adhesion and transport. Langmuir 20 (18), 7736–7746.
Walker, S.L., Redman, J.A., Elimelech, M., 2005. Influence of growth phase on bacterial deposition: interaction mechanisms in packed-bed column and radial stagnation point flow systems. Environmental Science & Technology 39 (17), 6405–6411.

Walker, S., Elimelech, M., Redman, J., 2006. Influence of growth phase on bacterial deposition: interaction mechanisms in packed-bed column and radial stagnation point flow systems (vol. 39, pg 6405, 2005). Environmental Science & Technology 40 (17), 5586.

Williams, M.M., Braun-Howland, E.B., 2003. Growth of *Escherichia coli* in model distribution system biofilms exposed to hypochlorous acid or monochloramine. Applied and Environmental Microbiology 69 (9), 5463–5471.

Wood, S.R., Kirkham, J., Shore, R.C., Brookes, S.J., Robinson, C., 2002. Changes in the structure and density of oral plaque biofilms with increasing plaque age. Fems Microbiology Ecology 39 (3), 239–244.

Wu, M.-Y., Sendamangalam, V., Xue, Z., Seo, Y., 2012. The influence of biofilm structure and total interaction energy on *Escherichia coli* retention by *Pseudomonas aeruginosa* biofilm. Biofouling 28 (10), 1119–1128.

Wullings, B.A., Bakker, G., van der Kooij, D., 2011. Concentration and diversity of uncultured *Legionella* spp. in two unchlorinated drinking water supplies with different concentrations of natural organic matter. Applied and Environmental Microbiology 77 (2), 634–641.

Xi, C.W., Marks, D., Schlachter, S., Luo, W., Boppart, S.A., 2006. High-resolution three-dimensional imaging of biofilm development using optical coherence tomography. Journal of Biomedical Optics 11 (3).

Zaidi, A.H., Bakkes, P.J., Krom, B.P., van der Mei, H.C., Driessen, A.J.M., 2011. Cholate-stimulated biofilm formation by *Lactococcus lactis* cells. Applied and Environmental Microbiology 77 (8), 2602–2610.